Advances in Nano Research, *Vol. 3, No. 2 (2015) 81-96*
DOI: http://dx.doi.org/10.12989/anr.2015.3.2.081

Structure and optical properties of vapor grown In_2O_3: Ga nano-/microcrystals

Diego León Sánchez[1], Jesús Alberto Ramos Ramón[2], Manuel Herrera Zaldívar[3], Umapada Pal[*2] and Efraín Rubio Rosas[4]

[1]*Facultad de Ciencias de la Electrónica, Universidad Autónoma de Puebla, 18 Sur y Av. San Claudio, Edif. 109, Puebla, Pue. 72570, Mexico*
[2]*Instituto de Física, Universidad Autónoma de Puebla, Apdo. Postal J-48, Puebla, Pue. 72570, Mexico*
[3]*Centro de Nanociencia y Nanotecnología, Universidad Nacional Autónoma de México, Ensenada, B.C. 22800, Mexico*
[4]*Centro Universitario de Vinculación y Transferencia de Tecnología (CUVyTT), Universidad Autónoma de Puebla, 24 Sur, C.U., Puebla 72570, Mexico*

(Received June 15, 2015, Revised June 30, 2015, Accepted July 2, 2015)

Abstract. Octahedral shaped single crystalline undoped and Ga-doped indium oxide nano-and microcrystals were fabricated using vapor-solid growth process. Effects of Ga doping on the crystallinity, defect structure, and optical properties of the nano-/microstructures have been studied using scanning electron microscopy, microRaman spectroscopy, transmission electron microscopy and cathodoluminescence spectroscopy. It has been observed that incorporation of Ga does not affect the morphology of In_2O_3 structures due to its smaller ionic radius, and similar oxidation state as that of In. However, incorporation of Ga in high concentration (~3.31 atom %) causes lattice compression, reduces optical band gap and defect induced CL emissions of In_2O_3 nano-/microcrystals. The single crystalline Ga-doped, In_2O_3 nano-/microcrystals with low defect contents are promising for optoelectronic applications.

Keywords: indium oxide; vapor-solid growth; Ga-doping; optical properties

1. Introduction

Indium oxide (In_2O_3), a wide band gap (3.55-3.76 eV) transparent semiconductor, has received considerable attention for its technological applications in optoelectronic devices such as solar cells (Li *et al.* 2003, Bielz *et al.* 2011, Guo *et al.* 2011), windows heaters (Hamberg *et al.* 1984), field-effect transistors (Zhang *et al.* 2003), flat-panel displays (Granqvist 1993, Hamburg *et al.* 1986), and ultra-sensitive toxic gas detectors (Li *et al.* 2006, Takeuchi *et al.* 1991, Liang *et al.* 2001, Gurilo *et al.* 2003). Indium oxide based transparent conducting oxides (TCOs) are widely used as key components of numerous display and photovoltaic devices. For example, tin-doped indium oxide (ITO) films have been distinctively employed as efficient TCOs on a massive scale for more than 25 years (Granqvist 1991). Apart from tin, several other metals like cadmium, zinc, and molybdenum have also been used as dopant for indium oxide thin films to enhance their

*Corresponding author, Professor, E-mail: upal@ifuap.buap.mx

 ISSN: 2287-237X (Print), 2287-2388 (Online)

electrical conductivity without significant sacrifice of optical transparency (Wang *et al.* 2001, Phillips *et al.* 1995, Karn *et al.* 2012, Yoshida *et al.* 2004, Meng *et al.* 2002, Meng *et al.* 2001). Typical ITO films have a sheet resistance of 10 Ω/square, which is inadequate for future technologies such as flat panel display. Increasing the thickness of ITO films to lower their sheet resistance leads to unacceptable light absorption. Although the required sheet resistance is attainable for TCOs by proper metal doping or controlling dopant concentration, for technological applications, like thin-film transistors (TFTs) (Park *et al.* 2012) and electrochromic windows (Warmsingh *et al.* 2012), there is a need for TCOs with better transparency across visible spectrum, especially in the green-blue region (van Deelen *et al.* 2012). On the other hand, for the application of TCOs as contacts for surface emitting lasers, they should be transparent in the infrared region, especially in the 1.0-1.5 μm range, where ITO is strongly absorbing (Trasferetti *et al.* 2002, Chao *et al.* 2012, Wang *et al.* 2009). Meeting these challenging goals requires a major improvement in the properties of materials utilized as TCO. Ga-doped indium oxide has seen to be an effective transparent conductive material (Cava *et al.* 1994, Phillips *et al.* 1994), generally with an inferior electrical conductivity, but superior optical transparency in blue and green spectral regions than that of ITOs. The electrical conductivity of Ga-doped thin films could be improved to the level of commercial ITOs without considerable compromise of their optical transparency just by increasing their thickness (Babar *et al.* 2008). While thin films of Ga-doped In_2O_3 have been envisaged as interesting material for applications as TCOs, in nanostructure forms, indium oxide based materials are promising building blocks for the fabrication of forthcoming electronic devices in nanoscale, chemical sensors (Zhang *et al.* 2003, Gurlo *et al.* 1997, Tang *et al.* 2014), electro-optic modulators, and biosensors (Curreli *et al.* 2005). In the recent past, several research groups have tried to fabricate doped and undoped indium oxide nanostructures using various growth techniques (Park *et al.* 2011, Lim *et al.* 2005). Using thermal evaporation method and $In/In_2O_3/Ga$ mixture as precursor, Chun *et al*. (2004) synthesized Ga-doped In_2O_3 nanowires on alumina substrates, observing a substantial reduction of band gap energy (E_g) due to Ga doping. Through vapor-liquid-solid (VLS) growth method, Mohamed *et al.* (2013) synthesized Ga-doped In_2O_3 nanowires using $In/In_2O_3/Ga_2O_3/Ga$ mixture as precursor. While through VLS, only a small amount of Ga could be incorporated into In_2O_3 nanostructures along with the reduction of band gap energy, a decrease in optical transmittance was noticed. Considering such contradictory literature reports, a thorough study of the optical properties of nano- and microstructures of Ga-doped In_2O_3 with varying Ga content is necessary to understand the role of Ga.

In the present study, we fabricated Ga-doped In_2O_3 nano- and microcrystals of octahedral morphology through vapor-solid (VS) method, to study the effects of Ga incorporation on their structure and optical properties. The morphology and crystallinity of the samples were studied using scanning electron microscopy (SEM), transmission electron microscopy (TEM) and microRaman spectroscopy. UV-Vis optical absorption and room temperature cathodoluminescence (CL) spectroscopy techniques were used to study their optical properties.

2. Experimental

Ga-doped In_2O_3 structures were grown by vapor-solid growth process through vapor transport in a single-zone high-temperature tube furnace, equipped with multiple gas supply facility. A mixture of indium (granular, 99.9% purity, 4 mm average particle size), graphite powder, and Ga (99.99%, splatter) in 10:5:*X* (*X*=0, 1, and 2) weight ratio was placed into an alumina boat (72 mm

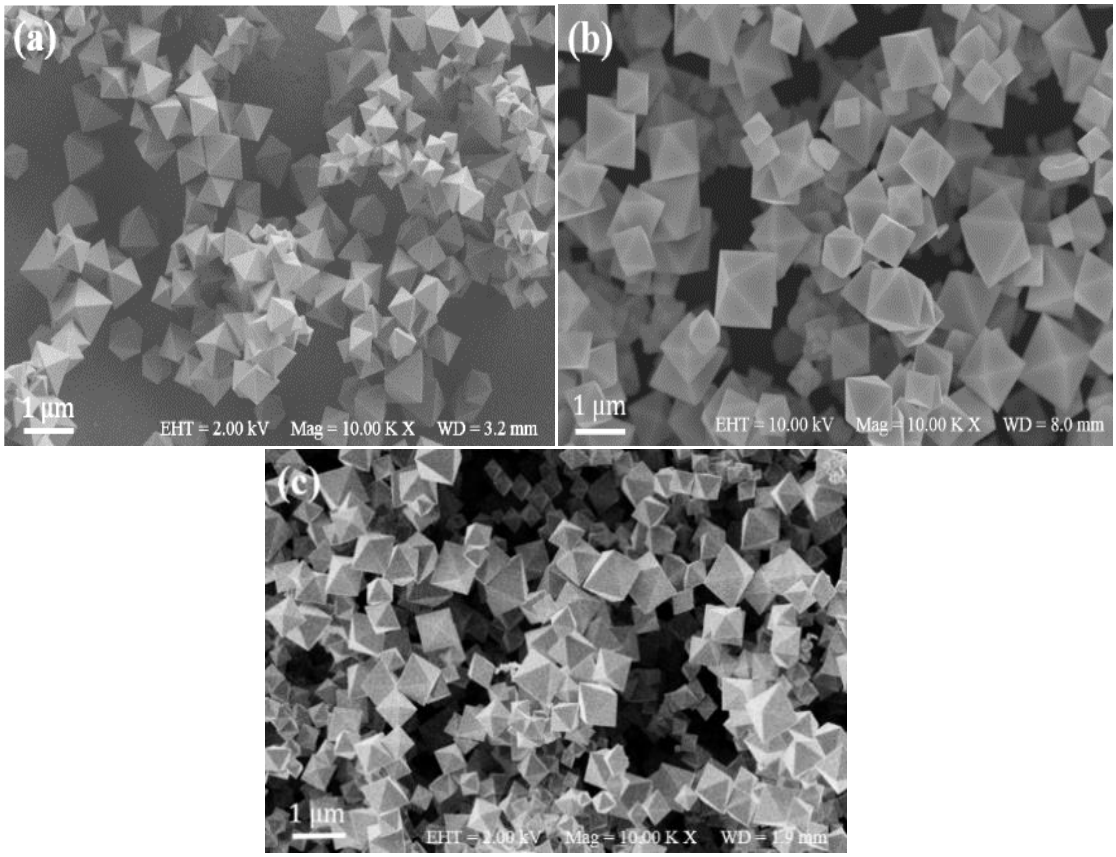

Fig. 1 Typical SEM images of (a) InGa-0, (b) InGa-1, and (c) InGa-2 samples showing the formation of octahedral particles with sharp facets and well-defined (nontruncated) tips

length) and kept at the center of a quartz tube (1.6 cm inner diameter, 114 cm length). The precursor-loaded quartz tube was then inserted into the horizontal tube furnace (Carbolite STF 15/180, max. temp. 1500℃) keeping the center of the quartz tube at the center of the furnace and fitted its two ends with the gas flow connectors. Before heating, a mixture of Ar (99.997%) and O_2 (99.999%) in 10:1 volume ratio was flown into the reaction tube for about 30 min. Then the precursor was heated to 1100℃ at a rate of 40℃/min, under a constant flow (220 sccm) of the gas mixture. A quartz substrate was placed at about 15 cm downstream of the source material, at a temperature of 700℃. After maintaining the maximum temperature at 1100℃ for 1h, the furnace was cooled down to room temperature naturally, and the white product deposited on the quartz substrate was collected. For the synthesis of undoped In_2O_3 structures, a mixture of In and graphite powder (weight ratio 2:1) was put into the alumina boat and the growth was performed under the same earlier mentioned experimental conditions. The samples prepared with 10:5:0, 10:5:1 and 10:5:2 weight ratios of indium, graphite, and gallium in the precursor mixture were designated as InGa-0, InGa-1, and InGa-2, respectively. The size, morphology and chemical composition of the nano/microstructures were examined in an AURIGA ZEISS high-resolution scanning electron microscope (HR-SEM) attached with Oxford analytical system. A JEOL JEM 2100F field emission transmission electron microscope (FE-TEM) attached with a charge coupled device

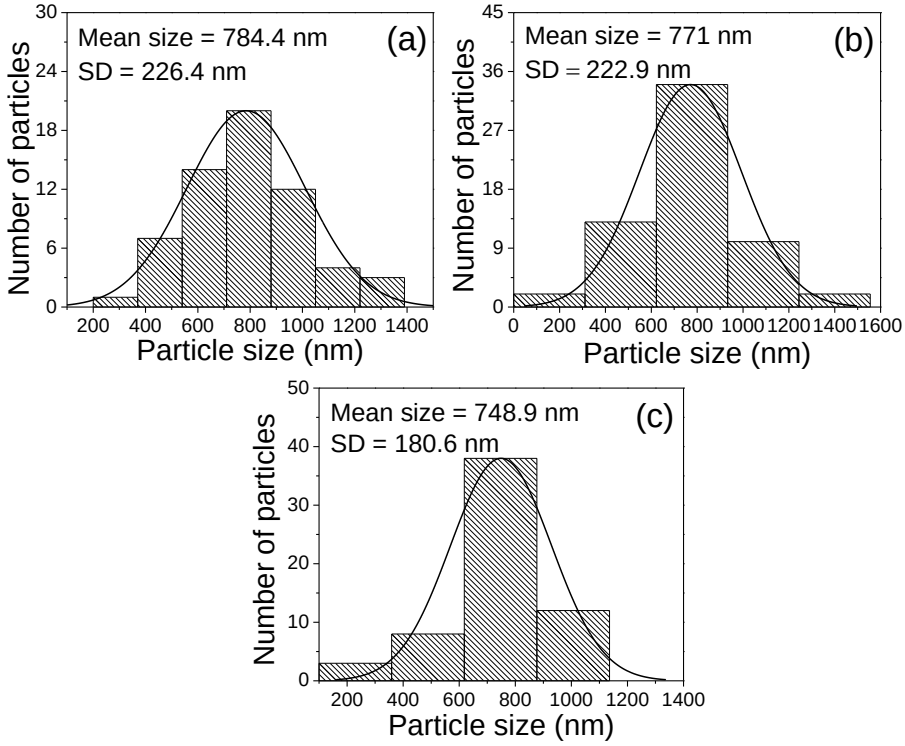

Fig. 2 Size distribution histograms and corresponding Gaussian fits for the (a) InGa-0, (b) InGa-1, and (c) InGa-2 samples

(CCD), operating at 200 kV, was utilized to study the morphology and crystal structure of the nanostructures. For TEM observations, the powder samples were dispersed in ethanol, spread over carbon coated microscopic grids, and dried in air at room temperature. Optical properties of the nano/microstructures were studied using microRaman spectroscopy (Horiba JOBIN-YVON spectrophotometer) in backscattering configuration using the 632.8 nm line of a He-Ne laser as excitation source, and UV-Vis optical absorption spectroscopy (SHIMADZU UV-3101PC) in the 190-1000 nm spectral range. The room temperature CL spectra of the doped and undoped samples were recorded in a JEOL JIB-4500 scanning electron microscope fitted with a Gatan mono-CL4 system.

3. Results and discussion

Fig. 1 shows typical SEM images of undoped and Ga-doped In_2O_3 particles, revealing the formation of octahedral shaped sub-micrometric particles for all the samples. As can be seen from the size distribution histograms presented in Fig. 2, the average size of the particles decreases gradually with the increase of Ga content. In order to verify the presence of Ga in the doped samples, both the doped and undoped samples were analyzed by energy dispersive spectroscopy (EDS). Typical EDS spectra and estimated composition of the samples are presented in Fig. 3 and

Table 1 EDS estimated composition of the undoped and Ga-doped In_2O_3 nano/microparticles. For EDS study, the nanoparticles were scratched out from the quartz substrate, and dispersed over Si wafer

Sample	Oxygen (at. %)	Indium (at. %)	Gallium (at. %)	In/O (at. ratio)	(In+Ga)/O (at. ratio)
InGa-0	69.28	30.32	0.0	0.44	0.44
InGa-1	73.51	26.10	0.39	0.36	0.36
InGa-2	73.23	23.46	3.31	0.32	0.36

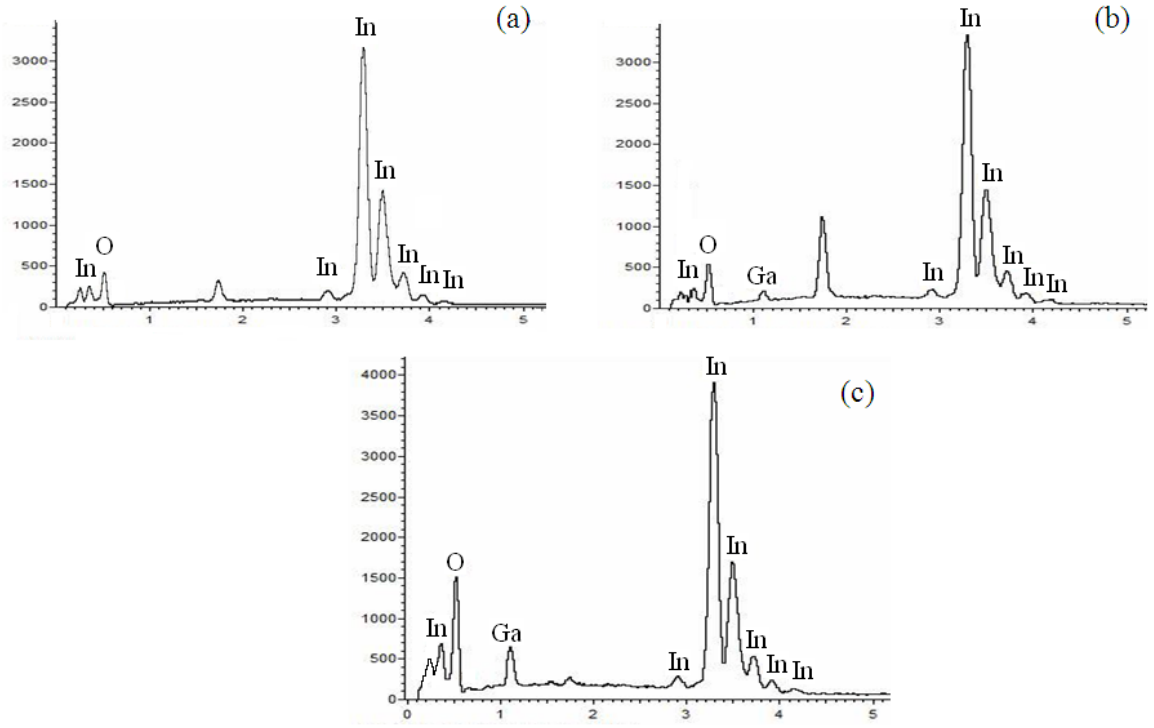

Fig. 3 Typical EDS spectra of (a) InGa-0, (b) InGa-1, and (c) InGa-2 samples. The peak centered at 1.74 keV corresponds to Si wafer used as support

Table 1, respectively. The EDS spectra of the doped samples clearly revealed the emission peaks correspond to O, In, and Ga. The amounts of incorporated Ga in the samples (Table 1) were considerably lower than their nominal values used in precursor mixtures. The low Ga content in the nanostructures was frequently attributed to the low solubility of Ga_2O_3 in In_2O_3 (<10 mol %) at growth temperatures in between 900 and 1000°C (D.D. Edwards *et al.* 1997, G. Patzke *et al.* 2000). As can be seen from Table 1, the atomic ratio In:O (~0.44) in the undoped sample is considerably lower than its stoichiometric value 0.66, indicating a deficiency of indium. On incorporating Ga in the nano/microstructures, this ratio decreased further to about 0.36 and 0.32 for the InGa-1 and InGa-2 sample, respectively. Both the indium oxide and Ga-doped indium oxide samples were grown under $Ar+O_2$ flow, which was stopped until the furnace was cooled down to room temperature. During this process, the formed nano/microstructures were

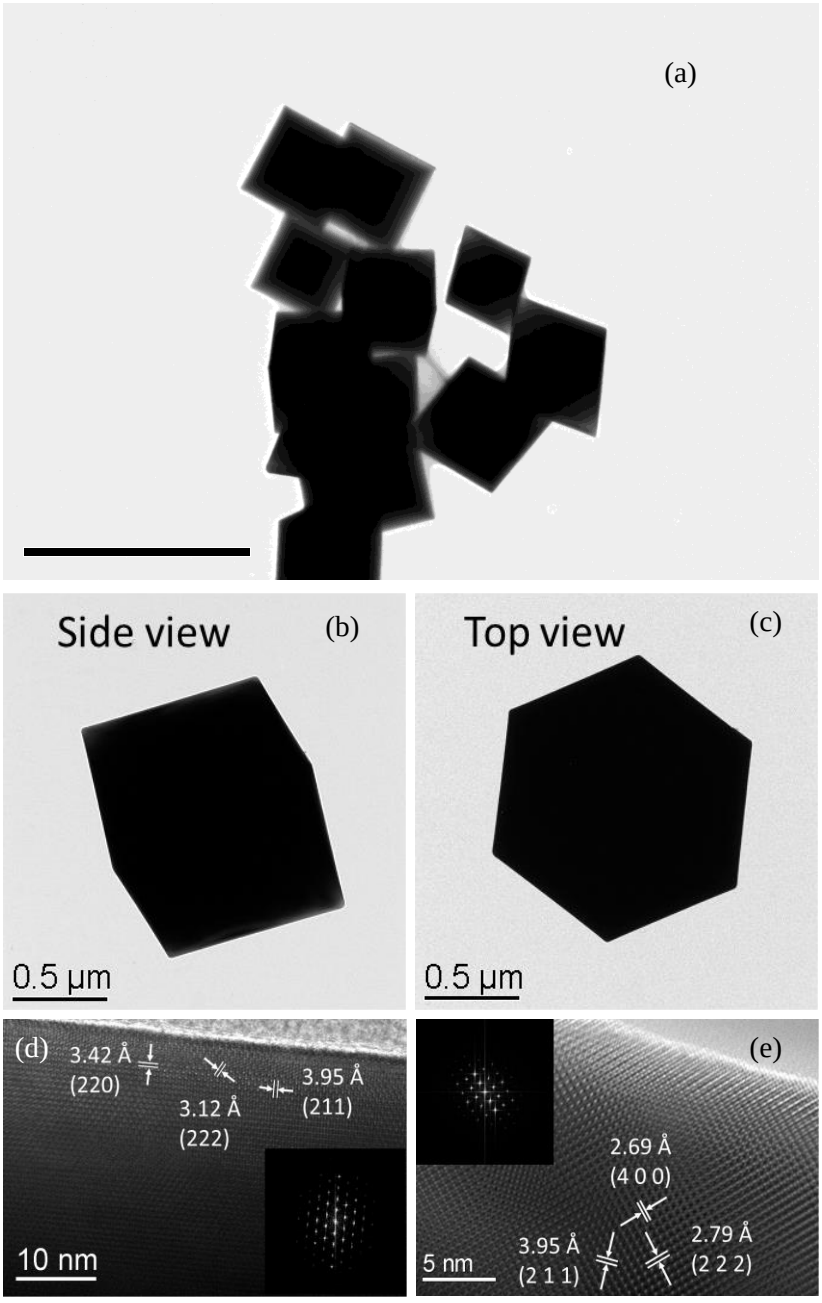

Fig. 4 Typical (a) low-resolution TEM image, (b) side view, and (c) top view of the same octahedral particle in undoped In_2O_3 sample. Typical HRTEM images of (d) InGa-0, and (e) InGa-2 samples showing their single crystalline nature. FFT patterns of selected areas for the samples are presented as insets

unintentionally annealed under oxygen atmosphere, partially filling up the inherent oxygen vacancies present in indium oxide (Ba *et al.* 2006). The further decrease of In:O atomic ratio in Ga-doped structures indicates additional oxygen incorporation due to Ga doping. On the other

hand, the gradual decrease of In content in the doped samples indicates that Ga incorporates in the nano/microstructures by substituting In in In_2O_3 lattice.

Fig. 4 presents typical low- and high-resolution TEM images of the undoped and Ga-doped In_2O_3 nano/microcrystal, reveling their octahedral morphology and crystalline structures. The high-resolution TEM (HRTEM) images of the periphery of the crystallites (Figs. 4(d) and 4(e)) revealed well-arranged crystalline planes of In_2O_3 in cubic phase (JCPDS# 88-2160). The single-crystal like nature of the particles is clearly manifested in the fast Fourier transformation (FFT) patterns of selected area of the HRTEM images presented as insets of Figs. 4(d) and 4(e). As can be noted from the typical HRTEM image of InGa-2 sample (Fig. 4(e)), incorporation of Ga as high as 3.31 atom % does not destroy the single crystalline nature of the particles. As expected from Vegard's law, the interplanar spacing reduces on the incorporation of Ga in indium oxide host lattice due the smaller ionic radius of Ga^{3+} compared to In^{3+} (Chun *et al.* 2004).

Effects of Ga doping on the crystallinity and lattice deformation of the In_2O_3 nanoparticles were also studied by recording their Raman spectra at room temperature (Fig. 5). Since the unit cell of cubic In_2O_3 lattice contains eight formula units, group theory predicts 120 vibrational modes for this structure following the representation (White *et al.* 1972)

$$\Gamma = 4A_g(R) + 4E_g(R) + 14T_g(R) + 5A_U + 5E_U + 17T_U(IR) \quad (1)$$

where E and T (also ascribed as F in the literature) modes are double and triple degenerated, respectively. While 22 gerade (g) modes are Raman-active (R), 16 T_u modes are infrared (IR) active; the A_u and E_u are silent modes, and the T_u mode corresponds to acoustic vibration (White *et al.* 1972, Wang *et al.* 2008). Unlike previous works (Korotcenkov *et al.* 2005, Matei *et al.* 2008), where a maximum of seven Raman modes have been observed, we observed ten Raman-active modes for In_2O_3 particles at room temperature. This difference in the number of Raman modes between previous works and ours might be associated to preparation processes and the nature of the sample. Most of the reported indium oxide samples are either polycrystalline thin films or powders annealed at high temperatures, where grain boundaries could break the symmetry rules and lead to quench some of the Raman modes. The Raman measurements are also sensitive to nanostructures morphology, as has been reported by Yin *et al*. (2009). The Raman spectra of our In_2O_3 particles (Fig. 5) revealed eight well-resolved bands with considerable intensities spreading through 110 to 707 cm^{-1} and two weak bands at about 119 and 154 cm^{-1}. The bands appeared around 110, 119, 154, 307, 367, 430, and 629 cm^{-1} have T_g symmetry, while the bands at 133, and 496 cm^{-1} have A_g symmetry. The bands appeared around 430 and 496 cm^{-1} have one shoulder each at around 450 and 520 cm^{-1}, respectively, which have T_{2g} symmetry (Kranert *et al.* 2014). The Raman band around 707 cm^{-1} has also been rarely observed in In_2O_3 (White *et al.* 1972), although least described in earlier studies. However, recently this band has been assigned to the cubic structure of In_2O_3 (Kim *et al.* 2007). The Raman spectrum of the undoped sample is dominated by the stretching modes near 133 cm^{-1} and 307 cm^{-1}. These same features are readily observed in the Ga-doped indium oxide samples, indicating the main contributions to the vibrational modes coming from the cubic In_2O_3 host lattice.

On Ga doping, while the intensity of the 307 cm^{-1} band decreased considerably, its full width at half maximum (FWHM) increased. Effects of Ga doping on the variation of these two parameters can be perceived clearly from Fig. 5 and Table 2. Both the decrease of intensity and increase of FWHM of the fundamental Raman bands for Ga-doped particles can be associated to the incorporation of Ga in In_2O_3 lattice. On the other hand, the position of the Raman band appeared around 133 cm^{-1} gradually shifted toward lower energy (lower wavenumber) on increasing the Ga

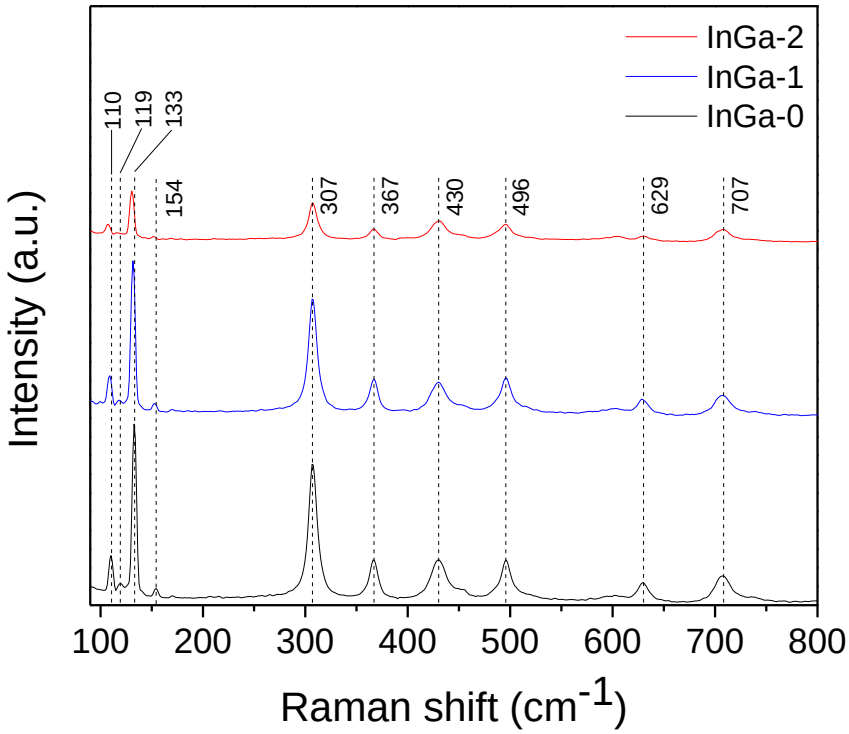

Fig. 5 Raman spectra of the undoped and Ga-doped In_2O_3 nano/microparticles

Table 2 Position and FWHM (in parenthesis) of the principal Raman bands for the undoped and Ga-doped In_2O_3 particles

	Position and FWHM (cm^{-1}) of Raman modes					
Sample	T_g	A_g	T_g	T_g	T_g	A_g
InGa-0	109.8 (3.1)	132.9 (3.6)	307.2 (11.3)	366.7 (10.0)	430.2 (17.1)	495.7 (14.1)
InGa-1	110.0 (3.2)	133.0 (3.7)	307.3 (11.4)	366.7 (9.9)	430.2 (17.4)	495.8 (15.5)
InGa-2	110.2 (3.8)	133.9 (4.2)	307.3 (11.6)	366.7 (10.2)	430.4 (18.7)	495.9 (19.2)

FWHM, full width at half maximum.

content in In_2O_3 crystals. The effect is prominent for the InGa-2 sample. The behaviors of 307 and 133 cm^{-1} Raman bands on Ga doping can be followed from the amplified spectra presented in Fig. 6. In Table II, the position and FWHM of the principal Raman bands revealed for the undoped and Ga-doped samples are summarized. The red shift of the 133 cm^{-1} band probably associated to the deformation caused by the incorporation of Ga in In_2O_3 lattice (Singhal *et al.* 2009). It is interesting to note that the Raman spectra of none of our samples revealed any band around 321 cm^{-1}, nor the observed 370 cm^{-1} band is asymmetric in shape, to indicate the nonstoichiometric nature of the samples (Zuo *et al.* 1994, McGuire *et al.* 2002) or the presence of high oxygen vacancy in them (White *et al.* 1972), respectively.

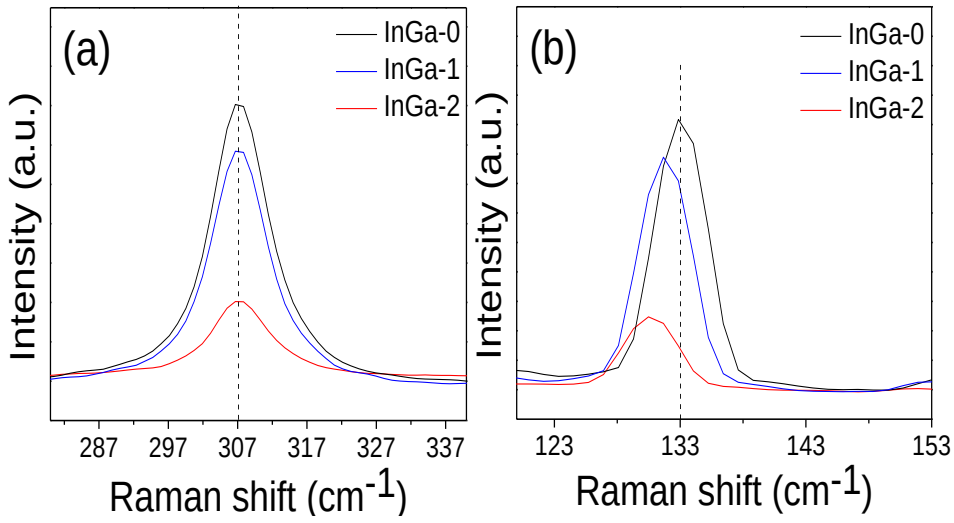

Fig. 6 Amplified Raman spectra of undoped and Ga-doped In_2O_3 samples showing a peak broadening and intensity reduction of the (a) 307 cm^{-1} and (b) red-shift of the 133 cm^{-1} Raman-active modes on Ga doping

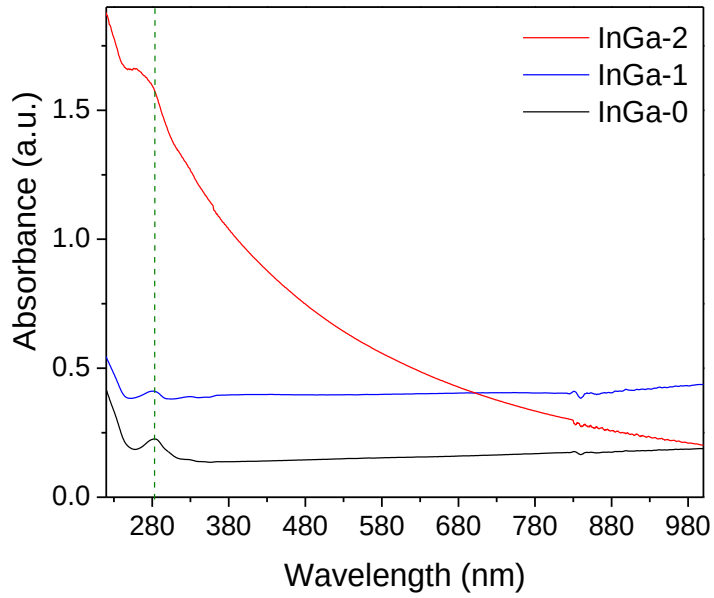

Fig. 7 UV-Vis absorption spectra of the undoped and Ga-doped In_2O_3 nano-/microparticles

The band gap energy of the undoped and Ga-doped indium oxide micro-/nanoparticles was determined from their optical absorption spectra in UV-Vis region at room temperature. For that, colloidal solutions of the samples were prepared by dispersing 1.5 mg of the powder sample (collected from the deposits over the quartz substrate) in 5 ml of ethanol. The absorption spectra (Fig. 7) of the colloidal samples were recorded in a SHIMDAZU UV-3100PC double-beam

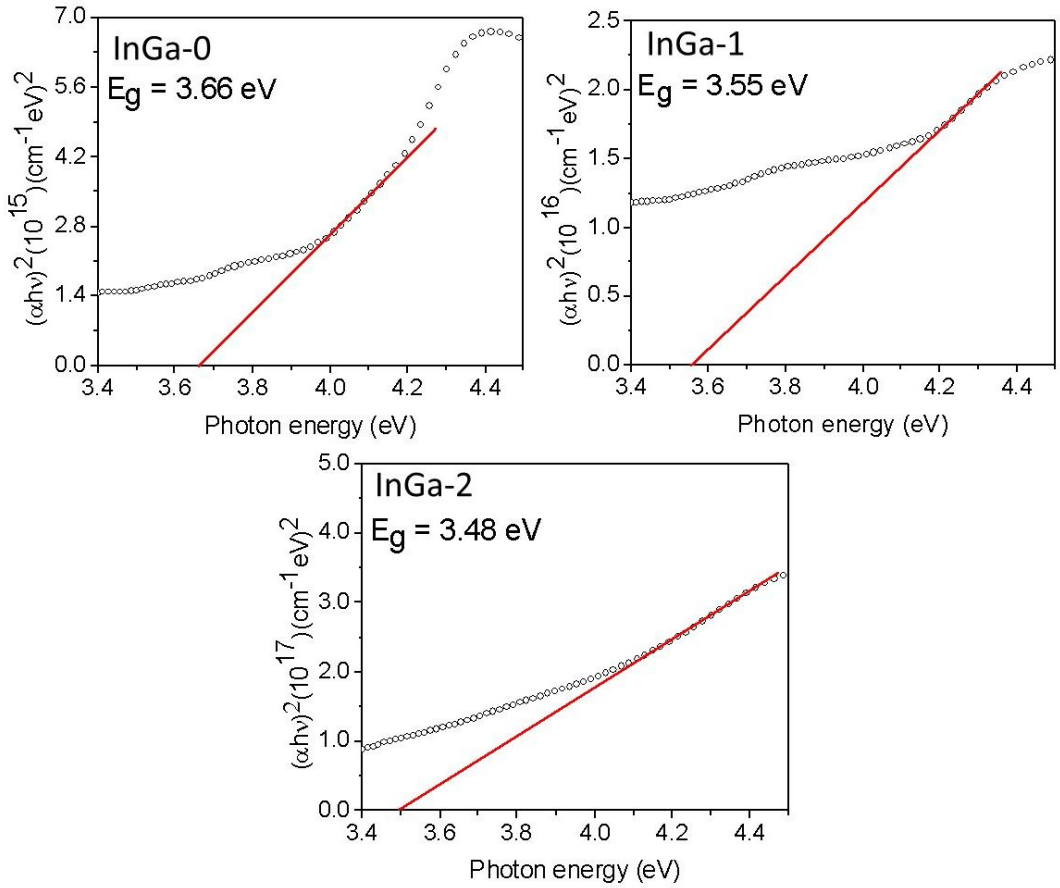

Fig. 8 $(\alpha h\nu)^2$ versus hν plots and band gap energy estimation of undoped and Ga-doped In_2O_3 nanoparticles for direct transition

spectrophotometer, utilizing ethanol as reference.

Absorption coefficients of the samples at different wavelengths were calculated from their absorption spectra utilizing the relation (Gu *et al.* 2002)

$$\alpha = \frac{2303A\rho}{lC} \tag{2}$$

where A is the absorbance; ρ is the density of In_2O_3; C is the concentration of the sample in solution; and l is the optical path length. The optical absorption coefficient α of a semiconductor close to its band edge can be expressed by the relation (Maensiri *et al.* 2006)

$$(\alpha h\nu)^n = K(h\nu - E_g) \tag{3}$$

where K is a constant, E_g is the band gap energy, and n is 2 or ½ depending on the nature (direct or indirect) of the transition. The band gap energies for the undoped and Ga-doped In_2O_3 samples were estimated from the $(\alpha h\nu)^2$ versus photon energy $(h\nu)$ plots, extrapolating the absorption coefficient values to the zero of the photon energy axis. The estimated band gap energy values

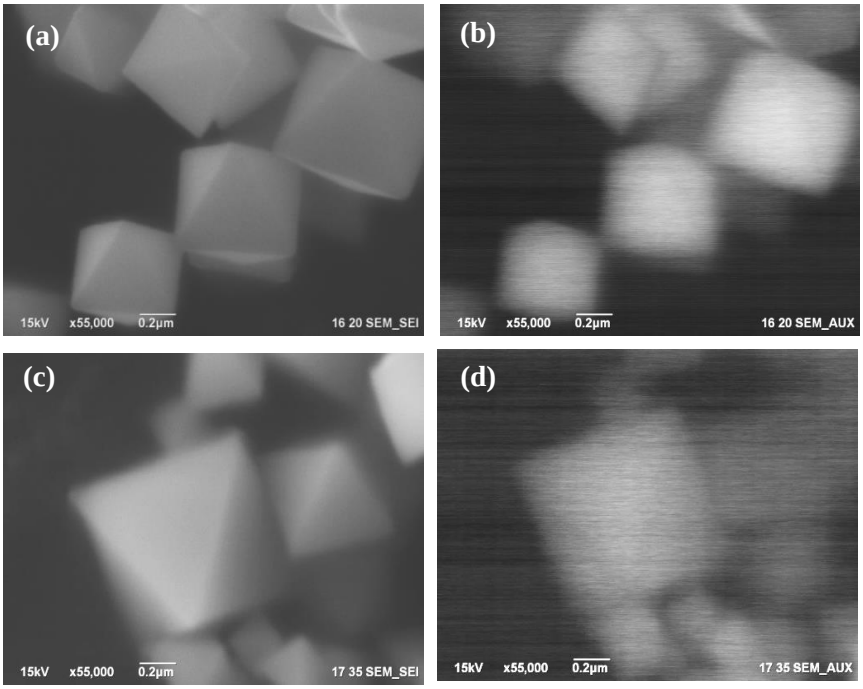

Fig. 9 SEM and CL images of (a)-(b) undoped (InGa-0), and (c)-(d) Ga-doped (InGa-1) In_2O_3 samples

were 3.66 eV, 3.55 eV and 3.48 eV for the InGa-0, InGa-1, and InGa-2 samples, respectively. It must be noted the absorption coefficient of the nano-/microstructures decreases gradually with the increase of Ga content in them (Fig. 8). The gradual decrease of E_g value on Ga incorporation into the In_2O_3 particles has been associated to the band bowing, that probably originates from the formation of localized band edge states due to charge exchange proportional to the orbital energy and structure relaxation, which is proportional to the size difference between Ga and In ions (Chun *et al.* 2004).

CL images of the InGa-0, InGa-1, and InGa-2 samples revealed homogeneous CL intensity distribution in the octahedral nano-/microparticles (Fig. 9) indicating the absence of dislocation and other non-radiative defects in them.

Room temperature CL spectra of the undoped and Ga-doped particles revealed an intense broad emission centered around 2.2 eV and a weak band at around 2.9 eV (Fig. 10). The intensity (integral) of CL emission is seen to decreases gradually on increasing the Ga content in the samples. Gaussian deconvolutions of CL spectra of the InGa-0 and InGa-1 samples revealed the presence of three component bands centered around 1.93 (orange band), 2.24 (green band) and 2.91 eV (blue band) (Figs. 10(a) and 10(b)). The origin of orange emission in In_2O_3 has not been clear so far. Recently it has been associated to the point defects generated by oxygen excess, such as interstitial oxygen (O_i), indium vacancies (V_{In}) or antisite oxygen (O_{In}) (Mazzera *et al.* 2007). On the contrary, several authors have associated orange band in In_2O_3 to the presence of oxygen vacancies (V_O) (Gao *et al.* 2006, Lee *et al.* 1996). The green emission has been observed in undoped In_2O_3 nanowires and nanoparticles (Zheng *et al.* 2001, Papageorgiou *et al.* 2011, Zhou *et al.* 1999), and associated to the formation of oxygen vacancies. Fig. 10(c) shows the CL spectrum of the InGa-2 sample, revealing a broad asymmetric emission with components centered around

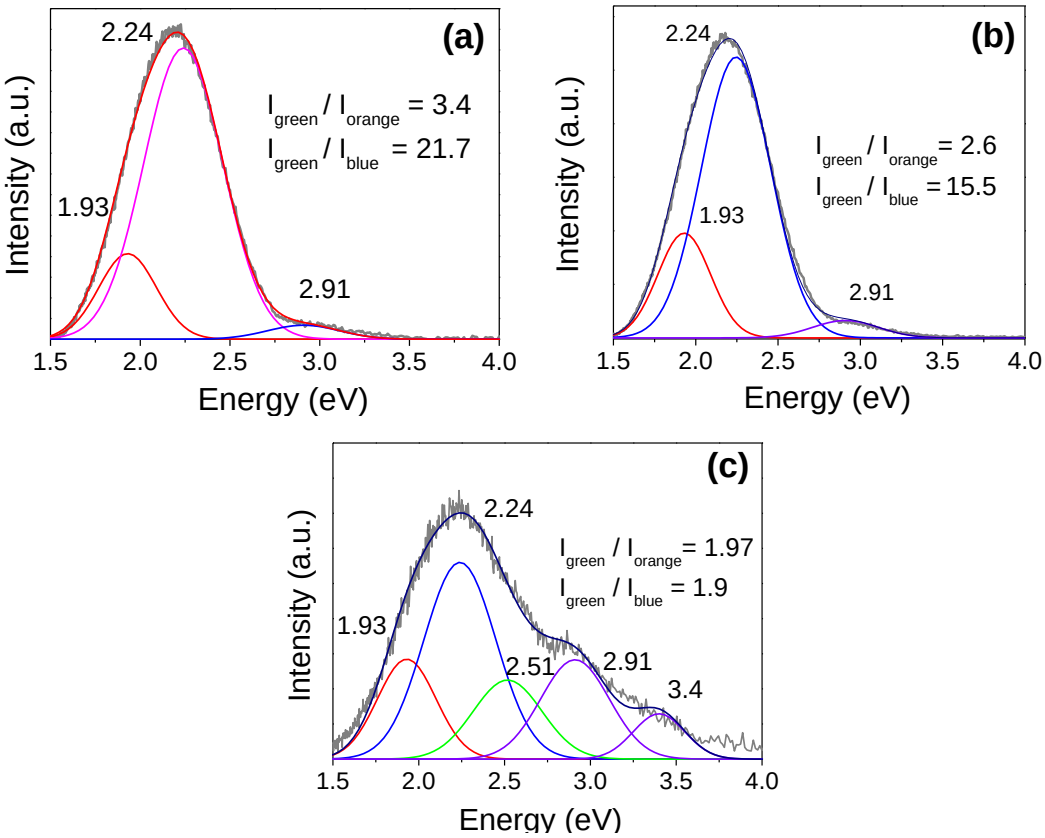

Fig. 10 Room temperature CL spectra of (a) InGa-0, (b) InGa-1, and (c) InGa-2 samples

1.93, 2.24, 2.51, 2.91 and 3.4 eV. Relative intensity of the green band decreases drastically on Ga incorporation in In_2O_3 lattice in high concentration. Quenching of the green emission due to Ga doping can be noticed clearly by comparing the intensity ratio I_{green}/I_{orange} in the samples. The I_{green}/I_{orange} ratios for the InGa-0, InGa-1 and InGa-2 samples were estimated to be of 3.4, 2.6 and 1.97, respectively. Similarly, the intensity ratio I_{green}/I_{blue} also decreases on increasing the Ga content in the samples, with values of 21.7, 15.5 and 1.9 (Fig. 10) for the InGa-0, InGa-1, and InGa-2 samples, respectively. As can be seen from the EDS results presented in Table 1, the amount of oxygen present in the micro-/nanostructures increases on increasing Ga content. These excess oxygen atoms fill up the oxygen vacancies (V_O) of the nanocrystals, which are inherently empty in undoped In_2O_3 (Li *et al.* 2004), reducing the defect-related emission in the CL spectra of the Ga doped micro-/nanostructures. The two component bands (Fig. 10(c)) appeared around 2.91 and 3.4 eV can been assigned to the near band edge emissions related to the indirect and direct band gap of In_2O_3, respectively (Girtan *et al.* 2005, el Hichou *et al.* 2009, Pramod *et al.* 2012). Finally, there appeared a component band in the blue-green region (around 494 nm or 2.51 eV) exclusively for the InGa-2 sample (Fig. 10(c)). Appearance of this band exclusively in the In_2O_3 structures with high Ga content indicates its association with Ga. In fact, Xu *et al.* (2007) have detected a PL (photoluminescence) emission at the same spectral position for their vapor grown hierarchical Ga_2O_3/In_2O_3 nanostructures containing hetero-junctions. Although they associated this emission to

In diffusion in Ga_2O_3 and creation of gallium vacancies, emissions close to this wavelength have also been observed in the PL and CL spectra of Ga-doped In_2O_3 and In-doped Ga_2O_3 nanostructures by several researchers, and been associated to oxygen vacancies and other defects (Wu *et al.* 2008, López *et al.* 2012).

4. Conclusions

In summary, single crystal In_2O_3 nano- and microparticles of octahedral shape could be synthesized successfully by vapor-solid growth process with different (up to 3.31 atom %) Ga contents. With limited solubility, most of the Ga atoms incorporate into In_2O_3 lattice substituting In atoms, without affecting its crystallinity. Incorporation of Ga in In_2O_3 nano-/microcrystals causes noticeable lattice compression, reduces band gap energy of direct transition, and reduces visible CL emission drastically. The intensity of defect-induced orange and green emission of In_2O_3 reduces on Ga incorporation, enhancing the relative intensity of near band emissions. The crystalline Ga-doped In_2O_3 nano- and microstructures with reduced defect content hold a great promise for the fabrication of future nanoscale optoelectronic devices.

Acknowledgements

The authors acknowledge the financial supports extended by CONACyT, Mexico (Grant # CB-2010/161767), and VIEP, BUAP (Grant # VIEP/EXC/2015), Mexico for realizing this investigation.

References

Ba, J., Fattakhova, D.F., Feldhaff, A., Brezesinski, T., Djerdj, I., Wark, M. and Niederberger, M. (2006), "Nonaqueous synthesis of uniform indium tin oxide nanocrystals and their electrical conductivity in dependence of the tin oxide concentration", *Chem. Mater*., **18**, 2848-2854.

Babar, A.R., Deshamukh, P.R., Deokate, R.J., Haranath, D., Bhosale, C.H. and Rajpure, K.Y. (2008), "Gallium doping in transparent conductive ZnO thin films prepared by chemical spray pyrolysis", *J. phys. D: Appl. Phys.*, **41**, 135404-125409.

Bielz, T., Lorenz, H., Amann, P., Klotzer, B. and Penner, S. (2011), "Water-gas shift and formaldehyde reforming activity determined by defect chemistry of polycrystalline In_2O_3", *J. Phys. Chem. C*, **115**, 6622-6628.

Cava, R.J., Phillips, J.M., Kwo, J., Thomas, G.A., Van Dover, R.B., Carter, S.A., Krajewski, J.J., Peck, W.F. Jr., Marshall, J.H. and Rapkine, D.H. (1994), "$GaInO_3$: A new transparent conducting oxide", *Appl. Phys. Lett.*, **64**, 2071-2072.

Chao, Y., Tang, W. and Wang, X. (2012), "Properties of resistivity, reflection and absorption related to structure of ITO films", *J. Mater. Sci. Technol.*, **28**(4), 325-328.

Chun, H.J., Choi, Y.S., Bae, S.Y., Choi, H.C. and Park, J. (2004), "Single-crystalline gallium-doped indium oxide nanowires", *Appl. Phys. Lett.*, **85**, 461-463.

Curreli, M., Li, C., Sun, Y., Lei, B., Gundersen, M.A., Thomson, M.E. and Zhou, C. (2005), "selective functionalization of In_2O_3 nanowire mat devices for biosensing applications", *J. Am. Chem. Soc.*, **127**(19), 6922-6923.

Edwards, D.D., Folkins, P.E. and Mason, T.O. (1997), "Phase equilibria in the Ga_2O_3-In_2O_3 system", *J. Am.*

Ceram. Soc., **80**(1), 253-257.
El Hichou, A., Addou, M., Mansori, M. and Ebothé, J. (2009), "Structural, optical and luminescent characteristics of sprayed fluorine-doped In_2O_3 thin films for solar cells", *Solar Ener. Mater. Solar Cell.*, **93**, 609-612.
Gao, T. and Wang, T. (2006), "Catalytic growth of In_2O_3 nanobelts by vapor transport", *J. Cryst. Growth*, **290**, 660-664.
Girtan, M. (2005), "Investigations on the optical constants of indium oxide thin films prepared by ultrasonic spray pyrolysis", *Mater. Sci. Technol. B*, **118**, 175-178.
Granqvist, C.G. (1991), "Solar energy materials: Overview and some examples", *Appl. Phys. A: Solid. Surf.*, **52**, 83-93.
Granqvist, C.G. (1993), "Transparent conductive electrodes for electrochromic devices: A Review", *Appl. Phys. A: Solid. Surf.*, **57**, 19-24.
Gu, F., Wang, S.F., Lü, M.K., Zhou, G.J., Xu, D. and Yuan, D.R. (2004), "Photoluminescence properties of SnO_2 nanoparticles synthesized by sol-gel method", *J. Phys. Chem. B*, **108**, 8119-8123.
Guo, L., Shen, X., Zhu, G. and Chen, K. (2011), "Preparation and gas-sensing performance of In_2O_3 porous nanoplatelets", *Sens. Actuators B*, **155**, 752-758.
Gurilo, A., Barsan, N., Weimar, U., Ivanovskaya, M., Taurino, A. and Siciliano, P. (2003), "Polycrystalline well-shaped blocks of indium oxide obtained by the sol-gel method and their gas-sensing properties", *Chem. Mater.*, **15**, 4377-4383.
Gurlo, A., Ivanovskaya, M., Barsan, N., Schweizer-Berberich, M., Weimar, U., Gopel, W., and Diéguez, A. (1997), "Grain size control in nanocrystalline In_2O_3 semiconductor gas sensors", *Sens. Actuat. B*, **44**, 327-333
Hamberg, I. and Granqvist, C. (1984), "Optical properties of transparent and heat reflecting indium tin oxide films: The role of ionized impurity scattering", *Appl. Phys. Lett.*, **44**, 721-723.
Hamburg, I. and Granqvist, C.G. (1986), "Evaporated Sn doped In_2O_3 films: Basic optical properties and applications to energy efficient windows", *J. Appl. Phys.*, **60**, R123-R159.
Karn, A., Kumar, M., Singh, V.N., Mehta, B.R., Aravindan, S. and Singh, J.P. (2012), "Growth of indium oxide and zinc-doped indium oxide nanostructures", *Chem. Vap. Deposition*, **18**, 295-301.
Kim, D.W., Hwang, I.S., Kwon, S.J., Kang, G.Y., Park, K.S., Choi, Y.J., Choi, K.J. and Park, J.G. (2007), "Highly conductive coaxial SnO_2-In_2O_3 heterostructured nanowires for Li ion battery electrodes", *Nano Lett.*, **7**, 3041-3045.
Korotcenkov, G., Brinzari, V., Ivanov, M., Cerneavschi, A., Rodriguez, J., Cirera, A., Cornet, A. and Morante, J. (2005), "Structural stability of indium oxide films deposited by spray pyrolysis during thermal annealing", *Thin Solid Film.*, **479**, 38-51.
Kranert, C., Schmidt-Grund, R. and Grundmann, M. (2014), "Raman active phonon modes of cubic In_2O_3", *Phys. Status Solidi RRL*, **8**, 554-559.
Lee, M.S., Choi, W.C., Kim, E.K., Kim, C.K. and Min, S.K. (1996), "Characterization of the oxidized indium thin films with thermal oxidation", *Thin Solid Film.*, **279**, 1-3.
Li C.,Zhang, D., Han, S., Liu, X., Tang, T. and Zhou C. (2003), "Diameter-controlled growth of single-crystalline In_2O_3 nanowires and their electronic properties", *Adv. Mater.*, **15**(2), 143-146.
Li, B.X., Xie, Y., Jing, M., Rong, G.X., Tang, Y.C. and Zhang, G.Z. (2006), "In_2O_3 hollow microspheres: Synthesis from designed $In(OH)_3$ precursors and applications in gas sensors and photocatalysis", *Langmuir*, **22**, 9380-9385.
Li, C., Fan, W., Lei, B., Zhang, D., Han, S., Tang, T., Liu, T., Liu, Z., Asano, S., Meyyappan, M., Han, J., and Zhou, C. (2004), "Multilevel memory based on molecular devices", *Appl. Phys. Lett.*, **84**, 1949-1951.
Liang, C.H., Meng, G.W., Lei, Y., Phillipp, F. and Zhang, L.D. (2001), "Catalytic growth of semiconducting In_2O_3 nanofibers", *Adv. Mater.*, **13**, 1330-1333.
Lim, J.H., Yang, E.J., Hwang, D.K., Yang, J.H., Oh, J.Y. and Park, S.J. (2005), "Highly transparent and low resistance gallium-doped indium oxide contact to p-type GaN", *Appl. Phys. Lett.*, **87**, 042109-1-042109-3.
López, I., Utrilla, A.D., Nogales, E., Méndez, B., Piqueras, J., Peche, A., Ramírez-Castellanos, J. and González-Calbet, J.M. (2012), "In-doped gallium oxide micro- and nanostructures: Morphology,

structure, and luminescence properties", *J. Phys. Chem. C*, **116**, 3935-3943.
Maensiri, S., Laokul, P. and Promarak, V. (2006), "Synthesis and optical properties of nanocrystalline ZnO powders by a simple method using zinc acetate dihydrate and poly(vinyl pyrrolidone)", *J. Cryst. Growth*, **289**, 102-106.
Matei Ghimbeu, C., Schoonman, J. and Lumbreras, M. (2008), "Porous indium oxide thin films deposited by electrostatic spray deposition technique", *Ceram. Intl.*, **34**, 95-100.
Mazzera, M., Zha, M., Calestani, D., Zappettini, A., Lazzarini, L., Salviati, G. and Zanotti, L. (2007), "Low-temperature In_2O_3 nanowire luminescence properties as a function of oxidizing thermal treatments", *Nanotechnol.*, **18**, 355707-355713.
McGuire, K., Pan, Z.W., Milkie, D., Menéndez, J. and Rao, A.M. (2002), "Raman studies of semiconducting oxide nanobelts", *J. Nanosci. Nanotechnol.*, **2**, 499-502.
Meng, Y., Yang, X.L., Chen, H.X., Shen, J., Jiang, Y.M., Zhang, Z.J. and Hua, Z.Y. (2001), "A new transparent conductive thin film In_2O_3:Mo", *Thin Solid Film.*, **394**, 219-223.
Meng, Y., Yang, X.L., Chen, H.X., Shen, J., Jiang, Y.M., Zhang, Z.J. and Hua, Z.Y. (2002), "Molybdenum-doped indium oxide transparent conductive thin films", *J. Vac. Sci. Technol. A*, **20**, 288-290.
Mohamed, S.H. (2013), "Transparent conductive gallium-doped indium oxide nanowires for optoelectronic applications", *J. Korean Phys. Soc.*, **62**, 902-905.
Papageorgiou, P., Zervos, M. and Othonos. A. (2011), "An investigation into the conversion of In_2O_3 into InN nanowires", *Nanoscale Res. Lett.*, **6**, 311-315.
Park, J.H., Choi, W.J., Chae, S.S., Oh, J.Y., Lee, S.J., Song, K.M. and Baik, H.K., (2011), "Structural and electrical properties of solution-processed gallium-doped indium oxide thin-film transistors", *Jpn. J. Appl. Phys.*, **50**, 080202-1-080202-3.
Park, J.H., Yoo, Y.B., Lee, K.H., Jang, W.S., Oh, J.Y., Chae, S.S., Choi, W.J. and Baik, H.K. (2012), "Role of alkaline-earth metal in solution-processed indium oxide based thin-film transistors", *Appl. Phys. Express*, **5**, 111101-1 -111101-3.
Patzke, G., and Binnewies, M. (2000), "Investigations in the β-Ga_2O_3:In_2O_3 system: Crystal growth of solid solutions", *Solid State Sci.*, **2**, 689-699.
Phillips, J.M., Cava, R.J., Thomas, G.A., Carter, S.A., Kwo, J., Siegrist, T., Krajewski, J.J., Marshall, J.H., Peck, W.F. Jr. and Rapkine, D.H. (1995), "Zinc-indium-oxide: A high conductivity transparent conducting oxide", *Appl. Phys. Lett.*, **67**, 2246-2248.
Phillips, J.M., Kwo, J., Thomas, G.A., Carter, S.A., Cava, R.J., Hou, S.Y., Krajewski, J.J., Marshall, J.H., Peck, W.F. Jr., Rapkine, D.H. and Van Dover, R.B. (1994), "Transparent conducting thin films of $GaInO_3$", *Appl. Phys. Lett.* **65**, 115-117.
Pramod, N.G., Pandey, S.N. and Sahay, P.P. (2012), "Structural, optical and methanol sensing properties of sprayed In_2O_3 nanoparticle thin films", *Ceram. Int.*, **38**, 4151-4158.
Singhal, A., Achary, S.N., Manjanna, J., Jayakumar, O.D., Kadam R.M. and Tyagi, A.K. (2009), "Colloidal Fe-doped indium oxide nanoparticles: Facile synthesis, structural, and magnetic properties", *J. Phys. Chem. C*, **113**, 3600-3606.
Takeuchi, M., Watanabe, Y. and Ozawa, S. (1991), "Gas-sensitive properties of ultrafine In_2O_3 particle layers prepared by gas evaporation technique", *Appl. Surf. Sci.*, **48**, 526-529.
Tang, Y. and Ma, J. (2014), "In_2O_3 nanostructures: synthesis and chlorobenzene sensing properties", *RSC Adv.*, **4**, 25692-25697.
Trasferetti, B.C., Davanzo, C.U. and Zoppi, R.A. (2012), "Infrared reflection-absorption characterization of TiO_2 films on ITO: detection of LO modes", *Electrochem. Commun.*, **4**, 301-304.
Van Deelen, J., Illiberi, A., Hovestad, A., Barbu, I., Klerk, L. and Buskens, P. (2012), "Transparent conducting materials: overview and recent results", *Proceedings of the SPIE, Thin Film Solar* **4**, California, U. S., SPIE, 8470.
Wang, A., Babcock, J.R., Edleman, N.L., Metz, A.W., Lane, M.A., Asahi, R., Dravid, V.P., Kannewurf, C.R., Freeman, A.J. and Marks, T.J. (2001), "Indium-cadmium-oxide films having exceptional electrical conductivity and optical transparency: Clues for optimizing transparent conductors", *Proc. Nat. Acad. Sci.*, **98**, 7113-7116.

Wang, C.Y., Dai, Y., Pezolt, J., Lu, B., Kups, T., Cimalla, V. and Ambacher, O. (2008), "Phase stabilization and phonon properties of single crystalline rhombohedral indium oxide", *Cryst. Growth Des.*, **8**, 1257-1260.

Wang, Y., Li, L., Chen, J., Song, Z., An, Y. and Zhang, Y. (2009), "Preparation and Properties of Infrared Transparent Conductive Thin Films", *Proceedings of the Green Chemistry in Research and Development of Advanced Materials*, MRS Proceedings.

Warmsingh, C., Yoshida, Y., Readey, D., Perkins, J., Parilla, P., Teplin, C., Kaydanova, T., Alleman, J., Gedvilas, L., Keyes, B., Gessert, T., Coutts, T. and Ginley, D. (2003), "Highly Conductive Textured Molybdenum Doped Indium Oxide Thin Films", *Proceedings of the NREL Conference*, Colorado, U.S.

White, W.B. and Keramidas, V.G. (1972), "Vibrational spectra of oxides with the C-type rare earth oxide structure", *Spectrochim. Acta A*, **28**, 501-509.

Wu, P., Li, Q., Zhao, C.X., Zhang, D.L., Chi, L.F. and Xiao, T. (2008), "SO_2 adsorption capacity of K_2CO_3-impregnated activated carbon as a function of K_2CO_3 content loaded by soaking and incipient wetness", *Appl. Surf. Sci.*, **255**, 3201-3207.

Xu, L., Su, Y., Li, S., Chen, Y., Zhou, Q., Yin, S. and Feng, Y. (2007), "Self-assembly and hierarchical organization of Ga_2O_3/In_2O_3 nanostructures", *J. Phys. Chem. B*, **111**, 760-766.

Yin, W., Su, J., Cao, M., Ni, C., Cloutier, S.G., Huang, Z., Ma, X., Ren, L., Hu, C. and Wei, B. (2009), "$In(OH)_3$ and In_2O_3 micro/nanostructures: Controllable NaOAc-assisted microemulsion synthesis and Raman properties", *J. Phys. Chem. C*, **113**, 19493-19499.

Yoshida, Y., Wood, D.M., Gessert, T.A. and Coutts, T.J. (2004), "High-mobility, sputtered films of indium oxide doped with molybdenum", *Appl. Phys. Lett.*, **84**, 2097-2099.

Zhang, D.H., Li, C., Han, S., Liu, X.L., Tang, T., Jin, W. and Zhou, C.W. (2003), "Electronic transport studies of single-crystalline In2O3 nanowires", *Appl. Phys. Lett.*, **82**(1), 112-114.

Zheng, M.J., Zhang, L.D., Li, G.H., Zhang, Y.Z. and Wang, X.F. (2001), "Ordered indium-oxide nanowire arrays and their photoluminescence properties", *Appl Phys Lett.*, **79**, 839-841.

Zhou, H., Cai, W. and Zhang, L. (1999), "Electroluminescence from n-In_2O_3: Sn randomly assembled nanorods/p-SiC heterojunction", *Appl. Phys. Lett.*, **75**, 495-500.

Zuo, J., Xu, C., Liu, X., Wang, C., Wang, C., Hu, Y. and Qian, Y. (1994), "Study of the Raman spectrum of nanometer SnO_2", *J. Appl. Phys.*, **75**, 1835-1836.

JL